Vector spatial solitons influenced by magneto-optic effects in cascadable nonlinear media

A. D. Boardman and K. Xie
Photonics and Nonlinear Science Group, Joule Laboratory, Department of Physics, University of Salford, Salford, M5 4WT, United Kingdom
(Received 10 May 1996)

The theory of vector spatial solitons in cascadable nonlinear media, bounded by magneto-optic material, is established. The main work is preceded by a discussion of the fundamental-harmonic wave phenomenon and four coupled equations for the system are established. A number of simulations are provided that illustrate both the vector nature of a quadratically nonlinear film, bounded by magneto-optic media and the crucial role of the magnetic field. It is demonstrated that the powerful polarization control exercised by the magnetic field suggests a number of interesting applications. [S1063-651X(97)10901-1]

PACS number(s): 42.65.Tg, 02.60.Lj, 42.60.Jf, 42.65.Jx

I. INTRODUCTION

Second-order nonlinearity is, traditionally, associated with second-harmonic generation [1], and was not, until recently, seen as a source of intensity-dependent phenomena. The rejection of second-order materials as envelope, or spatial, soliton hosts appears to have been centered upon a linear phase-matching argument. This view has now changed [2–12], and the back-mixing, or down-mixing, which is called cascading, of the second harmonic, with the fundamental wave to create usable third-order nonlinearity in the form of an intensity-dependent refractive index, is opening up exciting prospects [13]. Featuring strongly among these are spatial soliton interactions [14–16]. Such excitations depend upon the competing roles of diffraction and nonlinearity and have already received some attention. The interaction between fundamental waves of angular frequency ω, with linear wave number k_ω, and harmonic waves, with angular frequency 2ω and linear wave number $k_{2\omega}$, can be understood in terms of a balance between nonlinear and linear phase mismatches. It is worthwhile to highlight this principle, using scalar waves for clarity of argument, therefore, before going on to investigate the more complex situation involving vector waves and magnetooptic effects.

Suppose that the scalar electric fields associated with ω and 2ω are E_ω and $E_{2\omega}$, respectively; then the frequency-domain amplitudes of the second-order nonlinear polarizations [13], in a material characterized by a susceptibility tensor $\chi^{(2)}_{ijk}$, are

$$P^{\mathrm{NL}}_{(0)}=\tfrac{1}{2}\chi^{(2)}(0,\omega,-\omega)E_\omega E^*_\omega, \tag{1a}$$

$$P^{\mathrm{NL}}_{(\omega)}=\tfrac{1}{2}\chi^{(2)}(\omega;2\omega,-\omega)E_{2\omega}E^*_\omega, \tag{1b}$$

$$P^{\mathrm{NL}}_{(2\omega)}=\tfrac{1}{2}\chi^{(2)}(2\omega;\omega,\omega)E_\omega E_\omega. \tag{1c}$$

ε_0 is not included in these formulas, where the dc term $P^{\mathrm{NL}}_{(0)}$ cannot act as a source term to generate waves, leaving only $P^{\mathrm{NL}}_{(\omega)}$ and $P^{\mathrm{NL}}_{(2\omega)}$ to act as drivers for interacting waves. Given that this is the case, the $(\omega,2\omega)$ interaction process for the scalar cw waves under consideration here, that are propagating along the z axis, is governed by the well-known equations [1]

$$\frac{dE_\omega}{dz}=-i\Gamma_1 E_{2\omega}E^*_\omega e^{-i\Delta kz}, \tag{2a}$$

$$\frac{dE_{2\omega}}{dz}=-i\Gamma_2 E^2_\omega e^{i\Delta kz}, \tag{2b}$$

where $\Gamma_2=(\omega/2cn_{2\omega})\chi^{(2)}(2\omega;\omega,\omega)$, $\Gamma_1=(\omega/4cn_\omega)\chi^{(2)}(\omega;2\omega,-\omega)$, and $\Delta k=k_{2\omega}-2k_\omega$ is the *linear* phase mismatch. The amplitudes $E_\omega(z)$, $E_{2\omega}(z)$ contain possible nonlinear phases $\phi_\omega(z)$ and $\phi_{2\omega}(z)$, respectively. The amplitudes will therefore be written as $E_\omega=F_\omega e^{-i\phi_\omega}$ and $E_{2\omega}=F_{2\omega}e^{-i\phi_{2\omega}}$, where the dependence upon z is now implicit. From these definitions, it is not difficult to establish the following equations:

$$\frac{d^2F_\omega}{dz^2}-2\left(\frac{d\phi_\omega}{dz}\right)^2F_\omega-\frac{1}{F_\omega}\left(\frac{dF_\omega}{dz}\right)^2+\Gamma_1\Gamma_2F^3_\omega+\Delta k\left(\frac{d\phi_\omega}{dz}\right)F_\omega=0, \tag{3a}$$

$$2\left(\frac{d\phi_\omega}{dz}\right)\left(\frac{dF_\omega}{dz}\right)+F_\omega\frac{d^2\phi_\omega}{dz^2}-\Delta k\frac{dF_\omega}{dz}=0, \tag{3b}$$

with similar ones being obtainable for $F_{2\omega}$ and $\phi_{2\omega}$. Equations (3) can now be made to reveal how the balance between the ω and 2ω waves is achieved. If the boundary condition is $E_{2\omega}(0)=0$, $E_\omega(0)\neq0$, then $(dF_\omega/dz)_0=0$ and $(d\phi_\omega/dz)_0=0$, so that Eq. (3b) gives

$$\left[-\left(\frac{d\phi_\omega}{dz}\right)+\frac{\Delta k}{2}\right]=\frac{\Delta k}{2}\frac{F^2_\omega(0)}{F^2_\omega(z)}, \tag{4}$$

so that, for perfect linear phase matching, i.e., $\Delta k=0$, $F_\omega=\mathrm{sech}(\sqrt{\Gamma_1\Gamma_2}z)$, $\phi_\omega=\pi/4$, $F_{2\omega}=\sqrt{\Gamma_2/\Gamma_1}\tanh(\sqrt{\Gamma_1\Gamma_2}z)$, $\phi_{2\omega}=0$, and the interaction is not periodic. This is the classic case in which the conversion of ω to 2ω is 100%, and conversion back to ω does not occur. The point to be made here is that there is no *steady-state* combination of $(\omega,2\omega)$ waves.

For cw waves, a second type of boundary condition can be created, however, by making $E_\omega\neq0$ and $E_{2\omega}\neq0$, initially, i.e., $E_\omega(0)=F_\omega(0)e^{-i\phi_\omega(0)}$ and $E_{2\omega}(0)=F_{2\omega}(0)e^{-i\phi_{2\omega}(0)}$.

In this case, a balance between the ω and 2ω waves can be imposed by demanding that $dF_\omega/dz=0$ and $dF_{2\omega}/dz=0$; i.e., if $F_\omega(z)=F_\omega(0)$ and $F_{2\omega}(z)=F_{2\omega}(0)$ at $z=0$, then they will always *remain* at that value. The conditions for this interesting stationary state are

$$2\phi_\omega(z)-\phi_{2\omega}(z)=\Delta kz, \tag{5a}$$

$$\frac{d\phi_{2\omega}}{dz}=\Gamma_2\frac{F_\omega^2(0)}{F_{2\omega}(0)}, \tag{5b}$$

$$F_{2\omega}(0)=\frac{\Delta k\pm\sqrt{(\Delta k)^2+8\Gamma_1\Gamma_2F_\omega^2(0)}}{4\Gamma_1}. \tag{5c}$$

Actually, these equations can also be found in the paper by Schiek [8], but one difference is that he worked entirely in the frequency domain. Another difference is that Schiek discusses the problem in terms of *suppressing* the 2ω wave, by using the boundary condition. While it is true that the boundary condition does eliminate the generation of $\omega\rightarrow2\omega$ it is, nevertheless, the case that *both* the ω and 2ω waves are still present in the interaction. If the nonlinear phase shifts are defined as $\beta_\omega=d\phi_\omega/dz$ and $\beta_{2\omega}=d\phi_{2\omega}/dz$, then Eq. (5a) shows that this second type of boundary condition creates a stationary state whenever the nonlinear phase mismatch $\Delta\beta=\beta_{2\omega}-2\beta_\omega$ exactly *balances* the linear phase mismatch $\Delta k=k_{2\omega}-2k_\omega$. A type-1 boundary condition is responsible for second-harmonic generation, therefore, and type 2 is responsible for stationary state propagation. In other words, the waves in the two types of initial conditions, start differently and end up differently, in the cw case. The situation changes for beams of finite size. For the type-1 boundary condition, which is $E_{2\omega}(0)=0$ and $E_\omega(0)\neq0$, two long-term behaviors can be easily seen. If $E_\omega(0)$ is below some threshold, then $E_{2\omega}(z)$ is still generated, but both $E_{\omega(z)}$ and $E_{2\omega}(z)$ radiate away, due to diffraction. If $E_\omega(0)$ is above some threshold value, however, the energy switches back and forth between the fundamental and the harmonic a few times but eventually energy is distributed between ω and 2ω to form a stationary, spatial solitonlike beam. This is a balanced state. Of course, $E_{2\omega}(0)$ can always be selected to prevent even initial relaxations shedding unwanted energy, and a stationary state can be formed immediately. When this happens, again, it is not that 2ω is suppressed, but that a combined $(\omega,2\omega)$ solitonlike beam is formed. In other words, it is the unwanted adjustments associated with using $E_\omega(0)\neq0$, $E_{2\omega}(0)=0$ as initial conditions, or not selecting $E_\omega(0)\neq0$, $E_{2\omega}(0)\neq0$ to give a stationary state, immediately, that is avoided when Schiek refers to suppression. The above discussion is not coming from the same direction as the work of Schiek [8], but it should be recognized that his equations, in the end, contain the *same* mathematical content. Having now established the basics in terms of ω and 2ω scalar waves that are balanced to form stationary solitonlike states, by compensating *exactly* for any *linear* phase mismatch with a *nonlinear* phase mismatch, it is important to consider vector solitons. This is done in this paper with an added effect gained from using a waveguide that has a linear magnetooptic cladding and substrate.

II. VECTOR AND MAGNETO-OPTIC FORMULATION

The dielectric medium is assumed to be dominated by second-order nonlinear polarizations $\mathbf{P}^{\mathrm{NL}}(\omega)$ and $\mathbf{P}^{\mathrm{NL}}(2\omega)$, and that *vector* electric fields $\mathbf{E}(\omega)=(E_x(\omega),E_y(\omega))$, $\mathbf{E}(2\omega)=(E_x(2\omega),E_y(2\omega))$ are being propagated along the z axis. The fundamental wave has an angular frequency ω, and the harmonic wave has an angular frequency 2ω. The presence of *linear* magneto-optic material [17] creates, in addition, the polarizations $\mathbf{P}^M(\omega)$ and $\mathbf{P}^M(2\omega)$. If c is the velocity if light in a vacuum, and $n(\omega)$ and $n(2\omega)$ are the *zero magnetic field, zero nonlinearity* and *linear* refractive indices at the respective ω and 2ω frequencies, then the general wave equations are

$$\nabla^2\mathbf{E}(\omega)-\nabla(\nabla\cdot\mathbf{E}(\omega))+\left(\frac{\omega}{c}\right)^2n^2(\omega)\mathbf{E}(\omega)+\left(\frac{\omega}{c}\right)^2\mathbf{P}^{\mathrm{NL}}(\omega)+\left(\frac{\omega}{c}\right)^2\mathbf{P}^M(\omega)=0, \tag{6a}$$

$$\nabla^2\mathbf{E}(2\omega)-\nabla(\nabla\cdot\mathbf{E}(2\omega))+\left(\frac{2\omega}{c}\right)^2n^2(2\omega)\mathbf{E}(2\omega)+\left(\frac{2\omega}{c}\right)^2\mathbf{P}^{\mathrm{NL}}(2\omega)+\left(\frac{2\omega}{c}\right)^2\mathbf{P}^M(2\omega)=0. \tag{6b}$$

The x components of the nonlinear polarizations are

$$P_x^{\mathrm{NL}}(\omega)=\tfrac{1}{2}[2\kappa_1E_x^*(\omega)E_x(2\omega)-2\kappa_2E_x^*(\omega)E_y(2\omega)-2\kappa_2E_y^*(\omega)E_x(2\omega)-2\kappa_1E_y^*(\omega)E_y(2\omega)], \tag{7a}$$

$$P_x^{\mathrm{NL}}(2\omega)=\tfrac{1}{2}[\kappa_1E_x^2(\omega)-\kappa_1E_y^2(\omega)-2\kappa_2E_x(\omega)E_y(\omega)], \tag{7b}$$

where the hexagonal and trigonal systems are covered and, therefore, the crystal classes 6, $6m2$, 32, and $3m$. The definitions of κ_1 and κ_2 are

$$2\kappa_1=\chi_{xxx}^{(2)}(\omega;-\omega,2\omega)=-\chi_{xyy}^{(2)}(\omega;-\omega,2\omega)=2\chi_{xxx}^{(2)}(2\omega;\omega,\omega)=-2\chi_{xyy}^{(2)}(2\omega;\omega,\omega), \tag{8a}$$

$$2\kappa_2=-\chi_{xyx}^{(2)}(\omega;-\omega,2\omega)=-\chi_{xxy}^{(2)}(\omega;-\omega,2\omega)=-\chi_{xxy}^{(2)}(2\omega;\omega,\omega). \tag{8b}$$

Similar expressions for the y components of $\mathbf{P}^{\mathrm{NL}}(\omega)$ and $\mathbf{P}^{\mathrm{NL}}(2\omega)$ can also be found.

The system under investigation is shown in Fig. 1, and consists of a film of quadratically nonlinear material which is bounded by a linear, magneto-optic, semi-infinite, cladding and substrate. Guide confinement is in the y direction and self-focusing, leading to spatial solitonlike stationary states, is along the x direction. The cladding and substrate are magnetized, with an external magnetic field, along the z axis. In this so-called longitudinal configuration the dielectric tensor of the cladding or substrate material is [18], for ω,

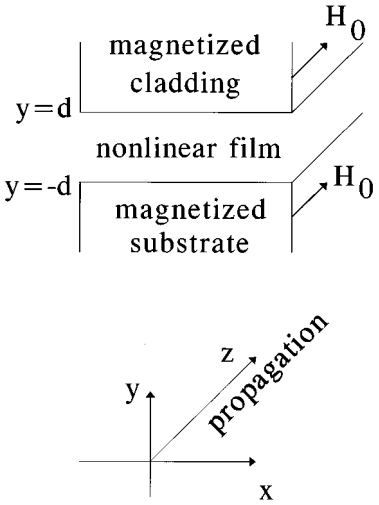

FIG. 1. The waveguide structure. H_0 is the applied magnetic field needed to activate the magneto-optical material. Both the cladding and the substrate are semi-infinite.

$$\underline{\underline{\varepsilon}}^{M}(\omega)=\begin{bmatrix} \varepsilon(\omega) & -iQ(\omega)\varepsilon(\omega) & 0 \\ iQ(\omega)\varepsilon(\omega) & \varepsilon(\omega) & 0 \\ 0 & 0 & \varepsilon(\omega) \end{bmatrix}, \quad (9)$$

and $\underline{\underline{\varepsilon}}^{M}(2\omega)$ has the same form. $Q(\omega)$ is a frequency-dependent magneto-optic coefficient which is induced by the applied magnetic field.

The polarization components, arising because of the magneto-optic nature of the substrate or cladding, are [17]

$$P_x^M(\omega)=-iQ(\omega)\varepsilon(\omega)E_y(\omega),$$

$$P_y^M(\omega)=iQ(\omega)\varepsilon(\omega)E_x(\omega), \quad (10a)$$

$$P_x^M(2\omega)=-iQ(2\omega)\varepsilon(2\omega)E_y(2\omega),$$

$$P_y^M(2\omega)=iQ(2\omega)\varepsilon(2\omega)E_x(2\omega), \quad (10b)$$

where it should be emphasized that the magneto-optic coupling parameter does, in principle, depend upon frequency. For many materials, the difference between $Q(\omega)$ and $Q(2\omega)$ will be slight, however. In the kind of waveguide that is typical for integrated optics the guiding is weak so that $\nabla(\nabla\cdot\mathbf{E}(\omega))\cong\mathbf{0}$, $\nabla(\nabla\cdot\mathbf{E}(2\omega))\approx\mathbf{0}$.

Suppose now that *average linear guiding* (zero magnetic field) wave numbers $k^{\omega}=\sqrt{(k_x^{\omega})^2+(k_y^{\omega})^2}/2$ and $k^{2\omega}=\sqrt{(k_x^{2\omega})^2+(k_y^{2\omega})^2}/2$ are introduced, where $k^{\omega}\neq\omega/c\sqrt{\varepsilon(\omega)}$ and $k^{2\omega}\neq\omega/c\sqrt{\varepsilon(2\omega)}$. The field components $E_{x,y}(\omega)$ and $E_{x,y}(2\omega)$ can then be expressed in the following, separable, form:

$$E_{x,y}(\omega)=\Gamma_{x,y}^{\omega}A_{x,y}^{\omega}(y)F_{x,y}(x,z)e^{ik^{\omega}z} \quad (11a)$$

$$E_{x,y}(2\omega)=\Gamma_{x,y}^{2\omega}A_{x,y}^{2\omega}(y)f_{x,y}(x,z)e^{ik^{2\omega}z}, \quad (11b)$$

where the normalization constants are

$$(\Gamma_x^{\omega})^2=\frac{1}{\int(A_x^{\omega})^2dy}\cong(\Gamma_y^{\omega})^2=\Gamma_{\omega}^2,$$

$$(\Gamma_x^{2\omega})^2=\frac{1}{\int(A_x^{2\omega})^2dy}\cong(\Gamma_y^{2\omega})^2=\Gamma_{2\omega}^2 \quad (12)$$

on the grounds that the cross-sectional modal areas, presented by $A_x^{\omega,2\omega}$ and $A_y^{\omega,2\omega}$, are very similar. The substitution of Eq. (11) into Eq. (6a), for example, gives

$$2ik^{\omega}\Gamma_{\omega}A_x^{\omega}\frac{\partial F_x}{\partial z}+\Gamma_{\omega}A_x^{\omega}\frac{\partial^2F_x}{\partial x^2}+\Gamma_{\omega}\frac{\partial^2A_x^{\omega}}{\partial y^2}F_x+\left[\left(\frac{\omega}{c}\right)^2n_x^2(\omega)-(k^{\omega})^2\right]\Gamma_{\omega}A_x^{\omega}F_x=0, \quad (13)$$

where

$$n_x^2(\omega)=[P_x^{\mathrm{NL}}(\omega)+P_x^M(\omega)]/E_x(\omega)+\varepsilon(\omega) \quad (14)$$

in which $\varepsilon(\omega)=n^2(\omega)$, and it should be recalled that $n(\omega)$ is the refractive index in the absence of both magnetic field and nonlinearity. Equation (13) can be treated by the method of separation, which involves splitting, through a separation constant k_x^{ω} into the two forms

$$2i\frac{k^{\omega}}{F_x}\frac{\partial F_x}{\partial z}+\frac{1}{F_x}\frac{\partial^2F_x}{\partial x^2}+[(k_x^{\omega})^2-(k^{\omega})^2]+[(\overline{k_x^{\omega}})^2-(k_x^{\omega})^2]=0, \quad (15a)$$

$$\frac{\partial^2A_x^{\omega}}{\partial y^2}+\left[\left(\frac{\omega}{c}\right)^2n_x^2(\omega)-(\overline{k_x^{\omega}})^2\right]A_x^{\omega}=0. \quad (15b)$$

The second equation is the nonlinear eigenmode equation. It will be used to generate $(k_x^{\omega})^2-(k_x^{\omega})^2$, which is needed for Eq. (15a). In the absence of nonlinearity and magnetic field, $k_x^{\omega}=k_x^{\omega}$, hence

$$\begin{aligned}F_x[(\overline{k_x^{\omega}})^2-(k_x^{\omega})^2]&=\frac{\omega^2}{c^2}\frac{\int[n_x^2(\omega)-\varepsilon(\omega)](A_x^{\omega})^2dy}{\int(A_x^{\omega})^2dy}F_x\\&=\left(\frac{\omega}{c}\right)^2[\overline{\kappa_1}F_x^*f_x-\overline{\kappa_2}F_x^*f_y\\&\quad-\overline{\kappa_2}F_y^*f_x-\overline{\kappa_1}F_y^*f_y]\\&\quad\times e^{i[k^{2\omega}-2k^{\omega}]z}-i\left(\frac{\omega}{c}\right)^2\overline{Q(\omega)\varepsilon(\omega)}F_y\end{aligned} \quad (16)$$

where $A_y^{\omega}\cong A_x^{\omega}$, and

$$\begin{aligned}\overline{\kappa_1}&=\Gamma_{2\omega}\frac{\int A_x^{2\omega}(A_x^{\omega})^2dy}{\int(A_x^{\omega})^2dy}\kappa_1\cong\Gamma_{2\omega}\frac{\int A_y^{2\omega}(A_x^{\omega})^2dy}{\int(A_x^{\omega})^2dy}\kappa_1\\&\approx\frac{\Gamma_{\omega}^2}{\Gamma_{2\omega}}\frac{\int(A_x^{\omega})^2A_x^{2\omega}dy}{\int(A_x^{2\omega})^2dy}\kappa_1\cong\frac{\Gamma_{\omega}^2}{\Gamma_{2\omega}}\frac{\int(A_y^{\omega})^2A_x^{2\omega}dy}{\int(A_x^{2\omega})^2dy}\kappa_1,\end{aligned} \quad (17a)$$

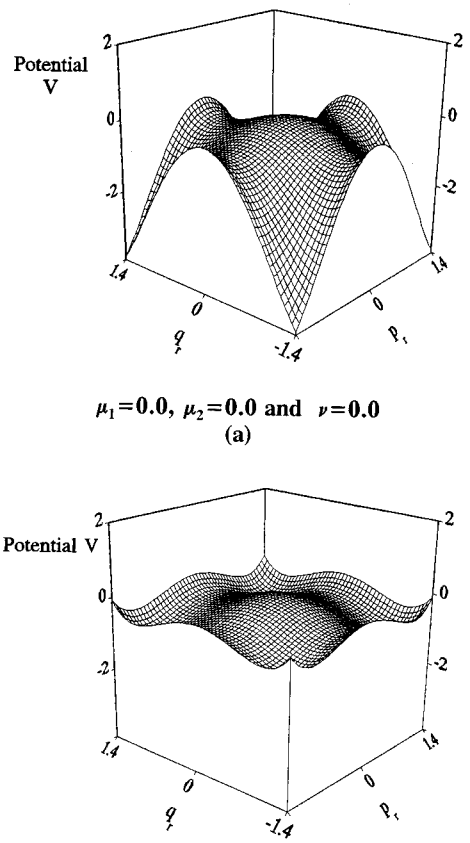

FIG. 2. The potential function $V(p_r, q_r)$ for $\mu_2=0$ and $\nu=0$, (a) $\mu_1=0$. (b) $\mu_1=1$.

$$\overline{\kappa_2}=\frac{\Gamma_\omega^2}{\Gamma_{2\omega}}\frac{\int A_x^\omega A_y^\omega A_x^{2\omega}dy}{\int (A_x^{2\omega})^2dy}\kappa_2 \cong \Gamma_{2\omega}\frac{\int A_y^{2\omega}(A_x^\omega)^2dy}{\int (A_x^\omega)^2dy}\kappa_2$$
$$\cong \Gamma_{2\omega}\frac{\int A_x^{2\omega}(A_x^\omega)^2dy}{\int (A_x^\omega)^2dy}\kappa_2, \tag{17b}$$

$$\overline{Q(\omega)\varepsilon(\omega)}=\frac{\int Q(\omega)\varepsilon(\omega)(A_x^\omega)^2dy}{\int (A_x^\omega)^2dy},$$
$$\overline{Q(2\omega)\varepsilon(2\omega)}=\frac{\int Q(2\omega)\varepsilon(2\omega)(A_x^{2\omega})^2dy}{\int (A_x^{2\omega})^2dy}. \tag{17c}$$

Equation (15a) becomes, therefore,

$$2ik^\omega\frac{\partial F_x}{\partial z}+\frac{\partial^2 F_x}{\partial x^2}+[(k_x^\omega)^2-(k^\omega)^2]F_x$$
$$-i\left(\frac{\omega}{c}\right)^2\overline{Q(\omega)\varepsilon(\omega)}F_y+\left(\frac{\omega}{c}\right)^2[\overline{\kappa_1}F_x^*f_x-\overline{\kappa_2}F_x^*f_y$$
$$-\overline{\kappa_2}F_y^*f_x-\overline{\kappa_1}F_y^*f_y]e^{i(k^{2\omega}-2k^\omega)z}=0. \tag{18}$$

If we now make the further transformations

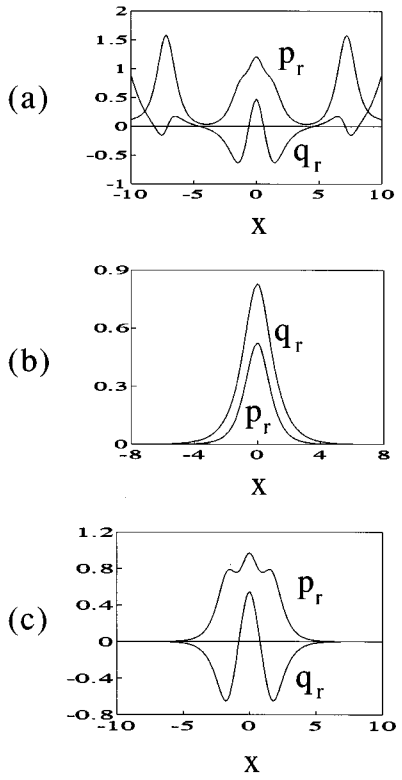

FIG. 3. Solutions p_r (dashed) and q_r (solid) as a function of x. (a) Example of a spurious (nonsensible) solution. (b) Symmetric solitonlike solution. (c) Multipeaked solitonlike solution. $\mu_1=1.0$, $\mu_2=0$, and $\nu=0$.

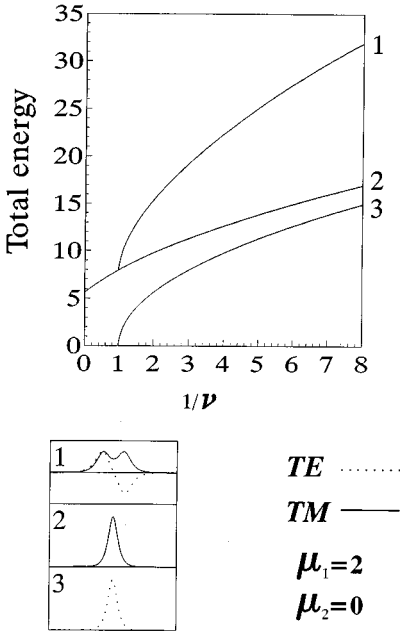

FIG. 4. Total energy of *combined* TE and TM modes as a function of $(1/\nu)$ $\mu_1=2$ and $\mu_2=0$. The solutions associated with branches 1, 2, and 3 are also shown.

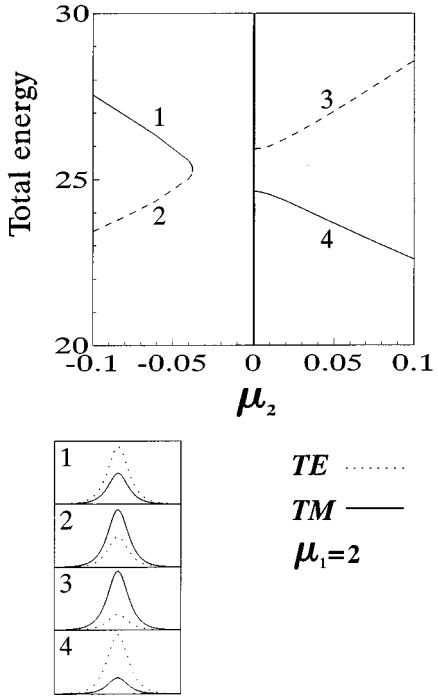

FIG. 5. Total energy of *combined* TE and TM modes as a function of μ_2. $\mu_1=2$ and $\nu=0$. The mode shapes for branches 1–4 are also shown.

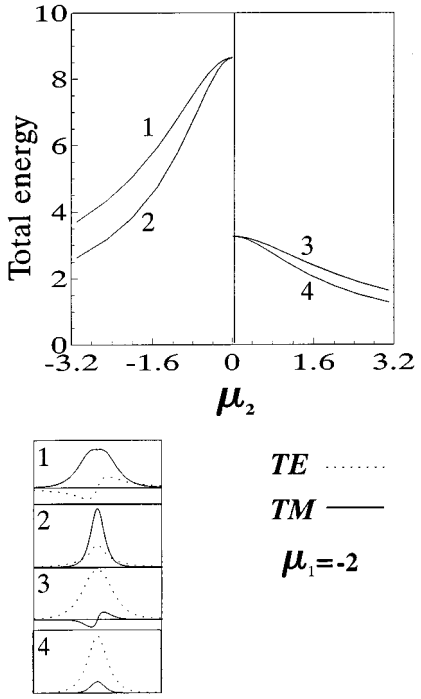

FIG. 6. Total energy of combined TE and TM modes as a function of μ_2 for a number of stationary states with $\mu_1=-2$ and $\nu=0$.

$$F_x=\frac{W_x}{\sqrt{2}}\exp(i\beta_1 z),\quad F_y=\frac{W_y}{\sqrt{2}}\exp(i\beta_1 z),\tag{19a}$$

$$f_x=V_x\exp(i\beta_2 z),\quad f_y=V_y\exp(i\beta_2 z),\tag{19b}$$

where β_1 and β_2 are nonlinear phase changes. Only soliton-like solutions are to be investigated here, so the choice $k^{2\omega}-2k^{\omega}+\beta_2-2\beta_1=0$ is made. After making $\beta_1 z\to z$ and $\sqrt{2k^{\omega}\beta_1}x\to x$, the following set of four coupled equations emerge:

$$i\frac{\partial W_x}{\partial z}+\frac{\partial^2 W_x}{\partial x^2}+\nu_1 W_x-W_x-iQ_1 W_y+\overline{\kappa_1}(W_x^* V_x-W_y^* V_y)-\overline{\kappa_2}(W_x^* V_y+W_y^* V_x)=0,\tag{20a}$$

$$i\frac{\partial W_y}{\partial z}+\frac{\partial^2 W_y}{\partial x^2}-\nu_1 W_y-W_y+iQ_1 W_x+\overline{\kappa_2}(W_y^* V_y-W_x^* V_x)-\overline{\kappa_1}(W_y^* V_x+W_x^* V_y)=0,\tag{20b}$$

$$2i\alpha\frac{\partial V_x}{\partial z}+\frac{\partial^2 V_x}{\partial x^2}+\nu_2 V_x-\alpha\beta V_x-iQ_2 V_y+\overline{\kappa_1}(W_x^2-W_y^2)-2\overline{\kappa_2}W_x W_y=0,\tag{20c}$$

$$2i\alpha\frac{\partial V_y}{\partial z}+\frac{\partial^2 V_y}{\partial x^2}-\nu_2 V_y-\alpha\beta V_y+iQ_2 V_x+\overline{\kappa_2}(W_y^2-W_x^2)-2\overline{\kappa_1}W_x W_y=0.\tag{20d}$$

Note that equations (19) also use the transformations

$$\left(\frac{\omega}{c}\right)^2\frac{W_{x,y}}{2k^{\omega}\beta_1}\to W_{x,y},\quad \left(\frac{\omega}{c}\right)^2\frac{V_{x,y}}{2k^{\omega}\beta_1}\to V_{x,y}$$

and the definitions

$$\nu_{1,2}=\frac{(k_x^{\omega,2\omega})^2-(k_y^{\omega,2\omega})^2}{4k^{\omega}\beta_1},\quad Q_1=\left(\frac{\omega}{c}\right)^2\frac{\overline{Q(\omega)\varepsilon(\omega)}}{2k^{\omega}\beta_1},$$

$$Q_2=\left(\frac{2\omega}{c}\right)^2\frac{\overline{Q(2\omega)\varepsilon(2\omega)}}{2k^{\omega}\beta_1},\quad \alpha=\frac{k^{2\omega}}{2k^{\omega}},\quad \beta=2\frac{\beta_2}{\beta_1},$$

where $\nu_{1,2}$ are birefringence parameters, and $Q_{1,2}$ are magnetooptic parameters.

The coupled equations (20) are not completely integrable but they do have, at least, three constants of motion. These are the following:

Effective mass (total energy)

$$M=-\frac{1}{\sqrt{2\pi}}\int[\tfrac{1}{2}|W_x|^2+\alpha|V_x|^2+\tfrac{1}{2}|W_y|^2+\alpha|V_y|^2]dx.\tag{21a}$$

Momentum

$$P=\frac{i}{\sqrt{2\pi}}\int\left[W_x\frac{\partial W_x^*}{\partial x}-W_x^*\frac{\partial W_x}{\partial x}+\alpha V_x\frac{\partial V_x^*}{\partial x}-\alpha V_x^*\frac{\partial V_x}{\partial x}+W_y\frac{\partial W_y^*}{\partial x}-W_y^*\frac{\partial W_y}{\partial x}+\alpha V_y\frac{\partial V_y^*}{\partial x}-\alpha V_y^*\frac{\partial V_y}{\partial x}\right]dx.\tag{21b}$$

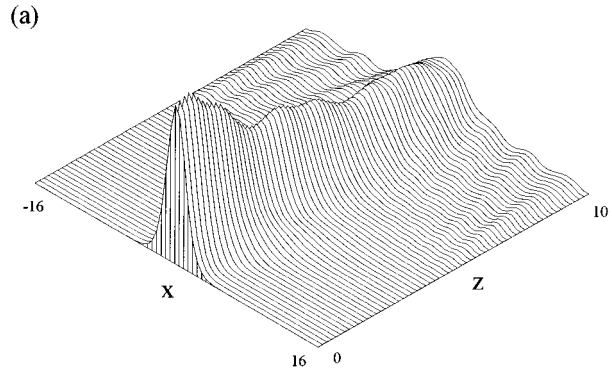

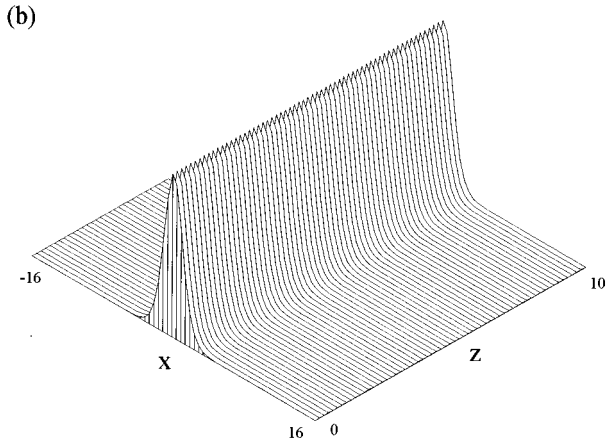

FIG. 7. Evolution from the TE input state $W_y = V_y = 0$ and $W_x = V_x = \frac{3}{2}\,\mathrm{sech}^2(x/2)$. (a) $6m2/3m$ crystal class with $\kappa_1 = 0$ and $\kappa_2 = 1$, (b) 32 crystal class with $\kappa_1 = 1$ and $\kappa_2 = 0$.

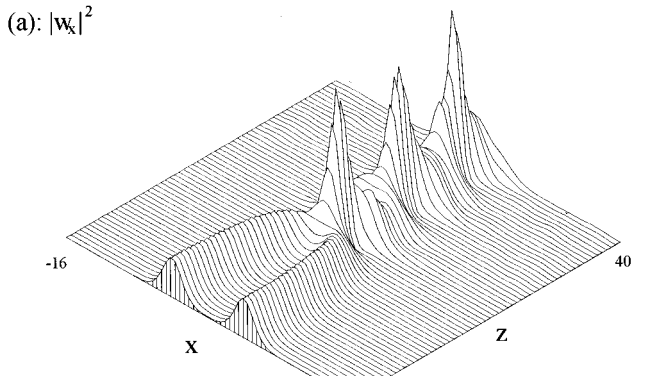

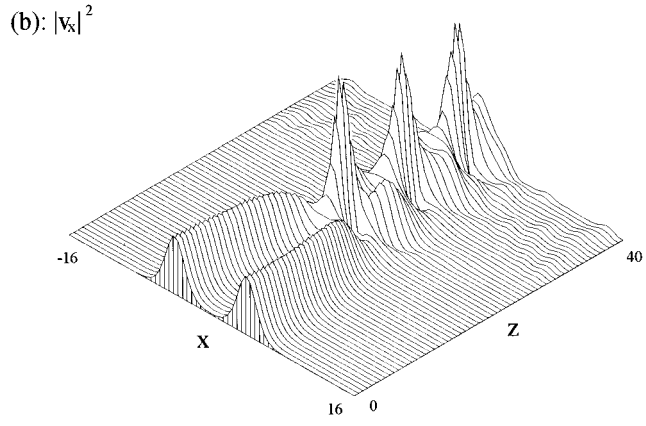

FIG. 8. Collision between two, initially, pure, in-phase, TE solitons with equal amplitudes, for a 32 crystal class. (a) W_x component. (b) V_x component. The W_y and V_y components are always zero, everywhere.

Hamiltonian

$$H=\left(\frac{2}{\pi}\right)^{1/2}\int\left[\left|\frac{\partial W_x}{\partial x}\right|^2+\left|\frac{\partial W_y}{\partial x}\right|^2+\frac{1}{2}\left|\frac{\partial V_x}{\partial x}\right|^2+\frac{1}{2}\left|\frac{\partial V_y}{\partial x}\right|^2-\nu_1|W_x|^2+\nu_1|W_y|^2-\frac{\nu_2}{2}|V_x|^2+\frac{\nu_2}{2}|V_y|^2+|W_x|^2+|W_y|^2+\frac{\alpha\beta}{2}|V_x|^2$$
$$+\frac{\alpha\beta}{2}|V_y|^2-iQ_1(W_xW_y^*-W_x^*W_y)-\frac{i}{2}Q_2(V_xV_y^*-V_x^*V_y)-\frac{\kappa_1}{2}(W_x^{*2}V_x+W_x^2V_x^*-2W_x^*W_y^*V_y-W_y^{*2}V_x-W_y^2V_x^*$$
$$-2W_xW_yV_y^*)-\frac{\kappa_2}{2}(W_y^{*2}V_y+W_y^2V_y^*-2W_y^*W_x^*V_x-W_x^{*2}V_y-W_x^2V_y^*-2W_yW_xV_x^*)\Bigg]. \tag{21c}$$

III. CASCADED LIMIT

In the cascaded limit, $\partial V_{x,y}/\partial z$ and $\partial^2 V_{x,y}/\partial x^2$ are negligible, so Eqs. (20c) and (20d) become

$$(\alpha\beta-\nu_2)V_x+iQ_2V_x=\kappa_1(W_x^2-W_y^2)-2\kappa_2W_xW_y,$$

$$-iQ_2V_x+(\alpha\beta+\nu_2)V_y=\kappa_2(W_y^2-W_x^2)-2\kappa_1W_xW_y$$

which have the solutions

$$V_x=D_x/D,\quad V_y=D_y/D,\quad D=\alpha^2\beta^2-\nu_2^2-Q_2^2,$$

and $D_{x,y}$ are the usual 2×2 determinants. The substitution of V_x and V_y into Eqs. (20a) and (20b) gives coupled equations for W_x and W_y. For example,

$$i\frac{\partial W_x}{\partial z}+\frac{\partial^2 W_x}{\partial x^2}+2\nu W_x+2|W_x|^2W_x-2W_x^*W_y^2$$
$$+2\mu_1|W_y|^2W_x+2\mu_2(W_x^2W_y^*-|W_y|^2W_y+2|W_x|^2W_y)$$
$$-iQ_1W_y-iQ_2(W_x^2W_y^*-|W_y|^2W_y-2|W_x|^2W_y)=0, \tag{22}$$

where $\nu=\nu_1/2$,

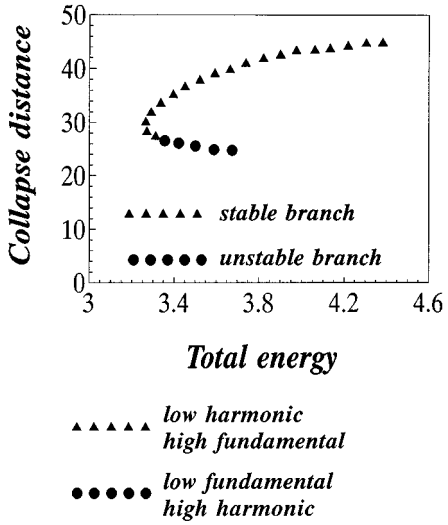

FIG. 9. Collapse distance, as a function of total energy for an interaction between two, initially, scalar solitons. The length curves, associated with the stable and unstable branches of the total energy curves are indicated, together with the fundamental and harmonic wave content.

$$\mu_1 = 2\frac{(\kappa_1^2+\kappa_2^2)\alpha\beta-(\kappa_1^2-\kappa_2^2)\nu_2}{(\kappa_1^2+\kappa_2^2)\alpha\beta+(\kappa_1^2-\kappa_2^2)\nu_2},$$

$$\mu_2 = \frac{-2\kappa_1\kappa_2\nu_2}{(\kappa_1^2+\kappa_2^2)\alpha\beta+(\kappa_1^2-\kappa_2^2)\nu_2},$$

$$\frac{2(\kappa_1^2+\kappa_2^2)Q_2}{(\kappa_1^2+\kappa_2^2)\alpha\beta+(\kappa_1^2-\kappa_2^2)\nu_2} \rightarrow Q_2,$$

and

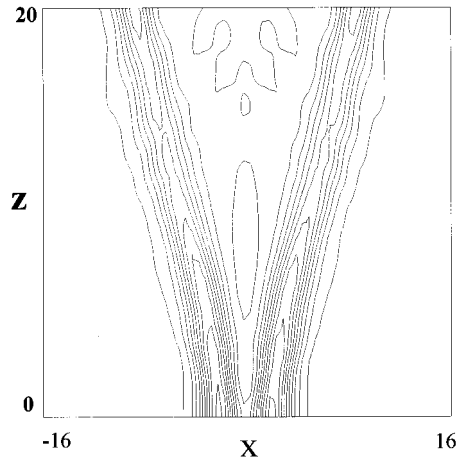

FIG. 10. Contour plot showing the cross section of the evolution of the interaction between an, initially, *scalar* TE soliton and a *pseudoscalar* soliton for a 32 crystal class. $\kappa_1=1$, $\kappa_2=0$, $Q_1=Q_2=0$, and $\nu_1=\nu_2=0$.

$$\left[\left(\frac{\kappa_1^2+\kappa_2^2}{2D}\,\alpha\beta+\frac{\kappa_1^2-\kappa_2^2}{2D}\,\nu_2\right)^{1/2}\right]W_{x,y}\rightarrow W_{x,y}\exp(-iz).$$

Stationary soliton solutions, in the form

$$\begin{aligned} W_x &= (p_r+ip_i)\exp(i2\lambda z), \\ W_y &= (q_r+iq_i)\exp(i2\lambda z), \end{aligned} \tag{23}$$

can now be looked for. Solutions (23), when used in Eq. (22), and the similar equation for W_y, give four coupled, ordinary, differential equations for the real and imaginary parts of the TE and TM field component amplitudes.

The numerical analysis begins with a simpler case, for which $\mu_2=0$. For a pure TE soliton solution, $p_i=q_r=q_i=0$ and $p_r=\rho\,\mathrm{sech}(\rho x)$, where $\rho^2=2(\lambda-\nu)$. This recovers the scalar case. Also $p_r=q_r=q_i=0$ and $p_i=\rho\,\mathrm{sech}(\rho x)$, where

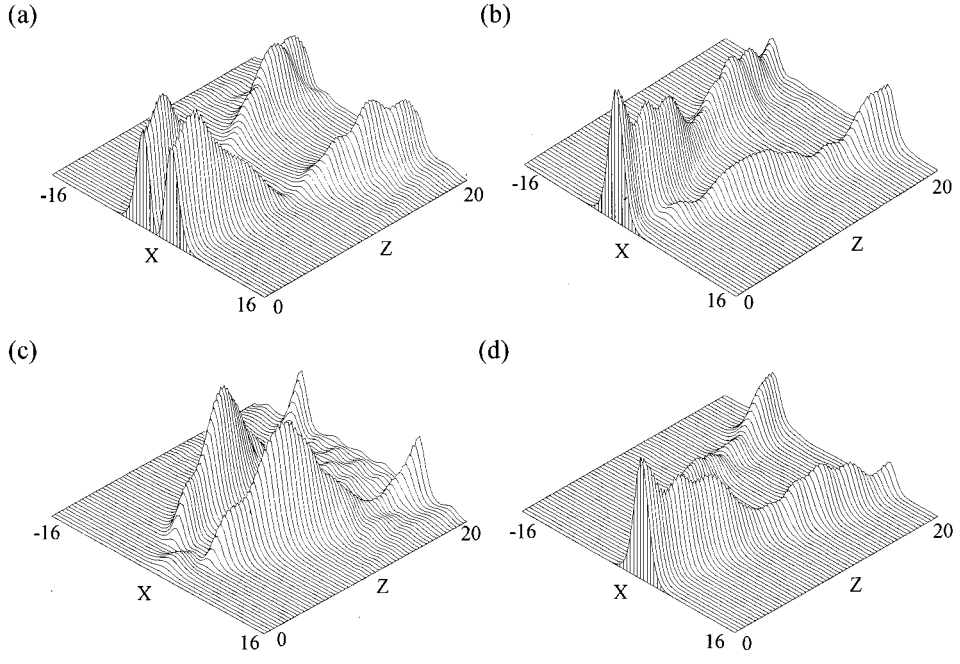

FIG. 11. Evolution of the four components of Fig. 10, showing that the wave component V_y is generated, shortly after the beam is launched. (a) V_x component. (b) W_x component. (c) V_y component. (d) W_y component. $\kappa_1=1$, $\kappa_2=0$, $Q_1=Q_2=0$, and $\nu_1=\nu_2=0$.

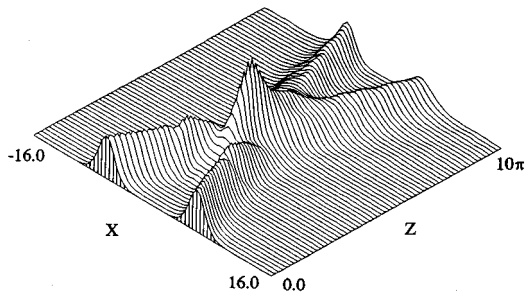

FIG. 12. Evolution of the interaction between two beams forced, initially, to be at an angle θ to each other. One beam sets out as a pure TE soliton [only $W_x \neq 0$, $V_x \neq 0$] and the other beam sets out as a pseudoscalar soliton [only $W_y \neq 0$, $V_x \neq 0$]. The crystal class is 32, so $\kappa_1 = 1$ and $\kappa_2 = 0$. Also $Q_1 = Q_2 = 0$ and $\nu_1 = \nu_2 = 0$.

ρ is the same as it is in the previous case. The solutions, however, have a $\pi/2$ phase shift with respect to each other. By the same logic, $q_r = \rho\,\mathrm{sech}(\rho x)$, with $\rho^2 = 2(\lambda + \nu)$ if $p_r = p_i = q_i = 0$, or $q_i = \rho\,\mathrm{sech}(\rho x)$, if $p_r = p_i = q_r = 0$.

The above solutions are scalar, and cease to exist if $\mu_2 \neq 0$. The coupled equations with $\mu_2 \neq 0$ have *vector* solutions, and it can be assumed that the solutions are real, i.e., $p_i = q_i = 0$ always. For example, the coupled equations can be reduced, via the transformations $\sqrt{\lambda}x \to x$, $\nu/\lambda \to \nu$, $(1/\sqrt{\lambda})p_r \to p_r$, and $(1/\sqrt{\lambda})q_r \to q_r$, to

$$\ddot{p}_r - 2(1-\nu)p_r + 2(p_r^2 - q_r^2)p_r + 2\mu_1 q_r^2 p_r + 2\mu_2(3p_r^2 - q_r^2)q_r = 0, \tag{24a}$$

$$\ddot{q}_r - 2(1+\nu)q_r + 2(q_r^2 - p_r^2)q_r + 2\mu_1 p_r^2 q_r - 2\mu_2(3q_r^2 - p_r^2)p_r = 0, \tag{24b}$$

where $\ddot{p}_r = d^2 p_r/dx^2$ and $\ddot{q}_r = d^2 q_r/dx^2$. These equations are integrable for $\mu_2 = 0$ and $\mu_1 = 2$, but, for other values, numerical simulations have to be generated. The Hamiltonian of the coupled equations (24a) and (24b) is

$$H = \tfrac{1}{2}(\dot{p}_r^2 + \dot{q}_r^2) - (p_r^2 + q_r^2) + \nu(p_r^2 - q_r^2) + \tfrac{1}{2}(p_r^2 - q_r^2)^2 + \mu_1 p_r^2 q_r^2 + 2\mu_2(p_r^2 - q_r^2)p_r q_r, \tag{25}$$

and the potential energy is

$$V(p_r, q_r) = -(p_r^2 + q_r^2) + \nu(p_r^2 - q_r^2) + \tfrac{1}{2}(p_r^2 - q_r^2)^2 + \mu_1 p_r^2 q_r^2 + 2\mu_2(p_r^2 - q_r^2)p_r q_r. \tag{26}$$

Figure 2 shows the forms of the potential function $V(p_r, q_r)$, for various values of μ_1, μ_2, and ν. The case for $\mu_1 = \mu_2 = 0.0$ and $\nu = 0.0$, is shown in Fig. 2(a), in which it can be seen that the trajectory of a ''particle'' on the potential surface evolves down a steep slope, and escapes to an infinity of q_r and p_r. No sensible solution is possible, therefore, for this system. For $\mu_1 = 1.0$, $\mu_2 = 0$, and $\nu = 0$ [Fig. 2(b)], however, sensible solutions are likely to occur, since any point on the surface that can evolve will remain at finite p_r and q_r values. Immediately, this kind of analysis shows that regular solutions are possible for p_r and q_r. Regular solutions can also exist for $\mu_1 = 1.0$, and small values of μ_2 and ν, since the potential is not modified so much that the dippedlike structure vanishes.

Equations (24) are ordinary differential equations and can be solved, numerically, with a technique known as the *shooting method* [19]. Solutions may appear during the numerical analysis, which do not make sense, but these can be rejected by using an iterative process to obtain convergence to an acceptable soliton result. Figure 3(a) shows such a nonsensible solution, but, in the class of meaningful solutions, two types are obtained, namely symmetric, and antisymmetric. Figure 3(b) shows stationary symmetric solutions for both p_r and q_r. Clearly, both p_r and q_r are *solitonlike solutions*. Other solitonlike solutions also exist, but these are multipeaked, as shown in Fig. 3(c). The p_r solution (dashed line)

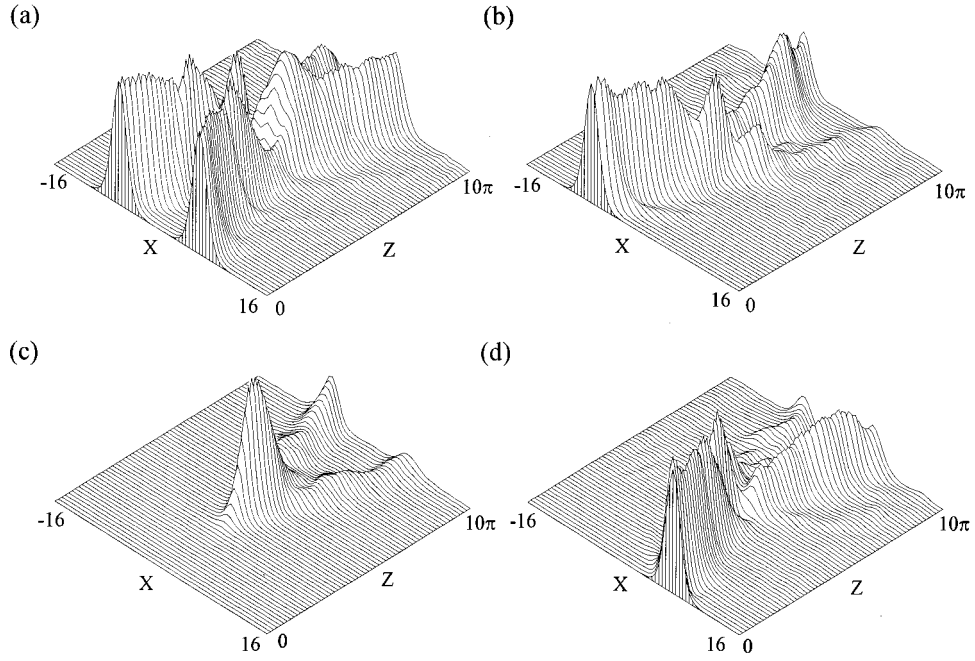

FIG. 13. (a) V_x, (b) W_x, (c) V_y, and (d) W_y components of the scalar-pseudoscalar interaction shown in Fig. 12. The peak of V_y is located at the collision point is clearly seen in this set of figures.

is similar, in this case, to a fundamental soliton, except that there is a slight bump at the top. On the other hand, the q_r solution (solid line) has negative values, and is multipeaked when the absolute value of the field is used. It is interesting that many more stationary state solutions exist.

The total energy of the two TE and TM modes, in the cascaded limit, as it changes with the parameters μ_1, μ_2 and ν, but with $Q_1=0$ and $Q_2=0$, will now be investigated. The total energy is defined as $E=(2/\sqrt{\nu})\int[(\sqrt{\lambda}p_r)^2+(\sqrt{\lambda}q_r)^2]d(x/\sqrt{\lambda})=(2/\sqrt{\nu})\int(p_r^2+q_r^2)dx$, and Fig. 4 shows that the total energy of the combined TE and TM modes is a function of the different initial profiles used. The parameters involved are $\mu_1=2$ and $\mu_2=0$. In Fig. 4 each number represents a typical curve for a particular solution to equations (25) which were found using the *shooting technique* [19]. Curves (1) and (2) coincide for large ν and split into two, as the birefringence parameter is reduced. The pure TM mode, represented by curve (2), has more energy, for the same birefringence parameter, than the mode of curve (3). Figure 5 shows what happens when the μ_2 parameter is varied, for the single-peaked structure. Curves (1) and (2) are in the same region, since they represent the same stationary profiles, except that the TE and TM modes have been switched around. For branches (1) and (2), branch (1) has a higher total energy than (2). They do coincide, however, for a particular value of μ_2, when μ_2 is about -0.035, but, as $|\mu_2|$ is increased, branch (1) increases in total energy, whereas branch (2) decreases. Branches (3) and (4) of Fig. 5 behave similarly, where branch (4) decreases in value, when the larger stationary solution is the TE mode, as with branch (1). Branch (3) increases in value, and the larger of the stationary solutions is TM. Here branches (3) and (4) do not meet like (1) and (2). When $\mu_2=0$, branches (3) and (4) reduce to pure TM and TE solutions, respectively. Figure 6 shows the total-energy variations, versus μ_2, for the single-peaked structure. It also shows the asymmetric stationary solutions, given by branches (1) and (3).

IV. NUMERICAL ANALYSIS OF THE FOUR COUPLED EQUATIONS

In Sec. III, the four coupled equations given by Eq. (20) were reduced to two, within the cascaded limit, and the scalar and vector solitons were examined as functions of ν, μ_1, and μ_2. Here some numerical computations of the four coupled equations are presented.

The numerical simulations have been carried out for a quadratically nonlinear material sandwiched between a semi-infinite, magneto-optic cladding and substrate. Since yttrium iron garnet (YIG) is transparent for 1.1–1.5-μm wavelengths, this material is selected to illustrate the effects. It is a well-known magnetic material, backed by a mature technology that has large enough off-diagonal elements in its dielectric tensor to produce easily measurable magneto-optic effects. A typical diffraction length is $L_D\cong 2.2$ mm. Typical beam widths $D_0\cong 8.5$ μm, and magneto-optic parameter $Q\sim 10^{-4}$ are also assumed. It is well-known that YIG can be saturated with a magnetic field $\sim$1750 G so that may be assumed. Also, the nonlinear film thickness is the order of 2 μm. To strike a note of caution, in principle, Q is a function of frequency, leading to Q_1 and Q_2, but it may also be a constant, or modulated with some function. For example, a modulation $\sin(\pi x/2)/|\sin(\pi x/2)|$ creates a periodic square function, which is perfectly possible from a technical point of view. The propagations will be allowed to proceed from $z=0$ to $z\cong 11$ cm and the transverse computational window is -68 μm$\leqslant x\leqslant 68$ μm.

For a certain crystal symmetry group, in the absence of an applied magnetic field, only solitons with a particular polarization state can be supported. For example, $\kappa_1=0$, in a crystal belonging to the $\overline{6m}2$, or $3m$ class. Pure TM ($W_y\neq 0$, $V_y\neq 0$) solitons can then propagate, while pure TE solitons ($W_x\neq 0$, $V_x\neq 0$) cannot. On the other hand, in a 32 class crystal, $\kappa_2=0$. In this case, pure TE solitons can propagate, but then pure TM solitons cannot. In a 6 class material, neither pure TE nor TM can propagate. In this case, a vector type of soliton, which is a mixture of TE and TM components, forms the *intrinsic* solution of the coupled equations.

Figure 7 shows the propagation of a pure TE soliton in different types of crystal. In the case $\kappa_1=0$, the field amplitude is normalized with κ_2, i.e., $\kappa_2 W_{x,y}\rightarrow W_{x,y}$ and $\kappa_2 V_{x,y}\rightarrow V_{x,y}$. In contrast, if $\kappa_2=0$, the field is normalized with κ_1. $\nu_1=\nu_2=0$, $Q_1=Q_2=0$, and $\alpha\beta=1$ are used here, and $W_x=V_x=\frac{3}{2}\,\mathrm{sech}^2(x/2)$ and $W_y=V_y=0$ are used at the input. Figures 7(a) and 7(b) show a pure TE soliton propagating in a $6m2/3m$ class crystal and 32 class crystal, respectively. For the reason mentioned above, solitons in Fig. 7(a) start radiating and decay soon after they are launched. A similar situation arises for a pure TM soliton, but for this solution, instead of decaying in a $6m2/3m$ crystal, it decays in a 32 class crystal.

Figure 8 shows a collision between, *initially*, two equal TE solitons in a 32 class crystal. Figures 8(a), 8(b), 8(c), and 8(d) display in the W_x, V_x, W_y, and V_y components, respectively. It is shown, in Figs. 8(c) and 8(d) that no TM component (W_y, V_y) is generated, in the collision. The collision is, nevertheless, inelastic, as the reduction in the oscillation period, and the small amount of radiation, indicate. This inelastic property of the collision originates from the fact that the coupled equations (20) do not have multisoliton solutions.

It is important to study interaction lengths, so, for the purpose of this calculation, the concept of *collapse length* is used. This is the distance through which the beams come to be overlapped by half their beam width. Using this definition, it can be seen in Fig. 9 that the collapse phenomenon is not as simple as it appears in Fig. 8. There are two branches to the collapse distance—total energy curves corresponding to stable and unstable states of the scalar soliton solution.

The stability of the scalar soliton solution of Eqs. (20), is discussed in [13]. One point that should be noted here, however, is that, if the growth rate of the unstable branch is very small, two solitons can collide, well before breakdown occurs. In such a case, a collapse length can still be defined. As the total energy increases, the growth rate of the unstable branch (lower branch in Fig. 9) increases, until the solitons lose their identity, before they meet each other. This is where the lower branch of Fig. 9 stops. Its upper branch will go on increasing forever. If the growth rate of the unstable branch is still rather small, the soliton will, nevertheless, radiate energy, immediately after it is launched. When a soliton encounters this radiation, it can ''see'' the existence of the

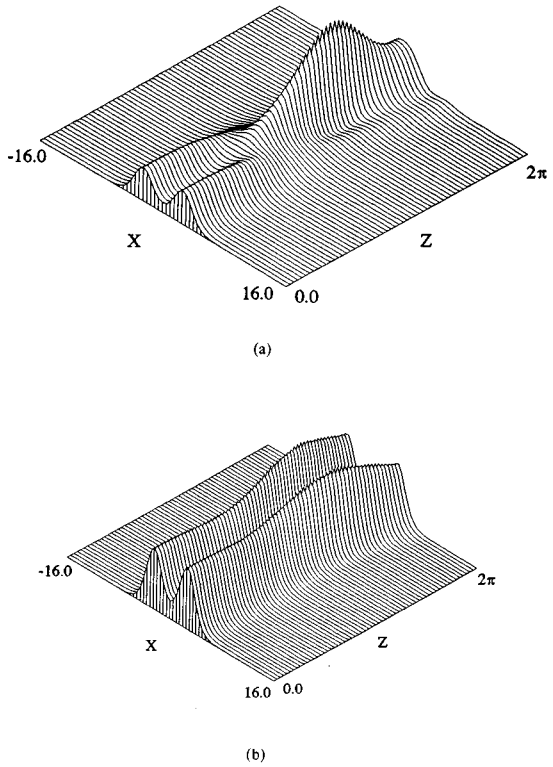

FIG. 14. Magneto-optic interaction of an, initially, TE soliton and a pseudoscalar soliton for $Q_1 \neq 0$ and $Q_2 = 0$. (a) $Q_1 = 0.2$, (b) $Q_1 = -0.2$.

other soliton, and their interaction is then enhanced. This radiation must be responsible for the shorter collapse length of the unstable solitons. For the 32 class ($\kappa_2 = 0$), a crystal cannot only support a pure scalar TE soliton ($W_x \neq 0$, $V_x \neq 0$, $W_y = 0$, $V_y = 0$), it can also support a pseudoscalar soliton ($W_x = 0$, $V_x \neq 0$, $W_y \neq 0$, $V_y = 0$). If $\nu_1 = \nu_2 = 0$ and $\alpha\beta = 1$, this pseudoscalar soliton solution is $W_x = V_y = 0$ and $W_y = -V_x = \frac{3}{2}\,\mathrm{sech}^2(x/2)$. The pure scalar TE soliton, in this case, is $W_y = V_y = 0$, $W_x = V_x = \frac{3}{2}\,\mathrm{sech}^2(x/2)$. The name ''pseudoscalar'' is clear when it is compared with the scalar TE soliton solution. The new solution has only two nonzero components, instead of four, so it should be called a scalar solution. But it is actually not a real scalar solution, because one of its nonzero components is polarized along $x(V_x)$ while the other nonzero components are polarized in the y direction (W_y). Similarly, a crystal of the $6m2$ or $3m$ class can support pure TM ($W_y \neq 0$, $V_y \neq 0$, $W_x = 0$, $V_x = 0$) solitons, and another type of pseudoscalar soliton solution ($W_x \neq 0$, $V_x = 0$, $W_y = 0$, $V_y \neq 0$).

Interaction between two pseudoscalar solitons is the same as TE-TE interactions. In Fig. 10 the interaction between a *scalar* TE soliton and a *pseudoscalar* soliton is shown for a 32 class crystal. The interaction shows repulsive behavior. Unlike the scalar TE-TE interaction, a wave component (V_y in this case) is generated, soon after the beam is launched, as shown in Fig. 11. This behavior can be used to make a polarization-generating device. Figure 11(c) shows that the generated V_y field reaches a maximum at a certain distance from the input, and then starts to decay. To make use of most of the generated V_y, the output must be near its maximum point. This maximum point, however, is difficult to monitor.

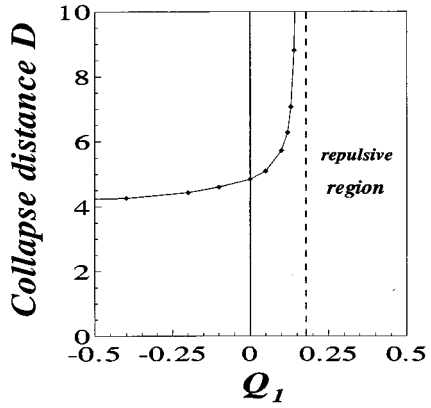

FIG. 15. Collapse distance for the interaction between an, initially, TE soliton and a pseudoscalar soliton, as a function of the magnetoptic parameter Q_1. Reversal of the applied magnetic field occurs when Q_1 changes sign.

One way to overcome this difficulty is to force the two beams to collide, by giving them an initial angle. Then the point where the generated V_y field reaches its maximum is always the point where the two beams collide. Figure 12 shows an example of this forced collision. There are two beams, and the one on the left is a pure TE soliton with only W_x and V_x components. The one on the right is a pseudoscalar soliton, and has only W_y and V_x components. Initially, they propagate at an angle to each other. Figures 13(a)–13(d) show its V_x, W_x, V_y, W_y components, respectively. Figure 13(a) shows the V_x collision and Fig. 13(d) shows the generation of V_x, with the V_y component being, initially, zero. As the beams pass through each other, energy is fed to it from other components, and it reaches its peak in the vicinity of the expected collision point, as shown in Fig. 13(c). Figures 13(b) and 13(d) show the W_x and W_y components, and it can be seen that the two sets of beams do not actually collide, but bounce off each other. In fact, each takes a slight shadow of its partner with it.

It is now an important question to see how the magnetic field alters this situation. As an example, consider the cases $Q_2 = 0$ and $Q_1 \neq 0$. Note that Q is the magneto-optic coefficient associated with the fundamental wave, and Q_2 characterizes the harmonic. Figure 14 shows two numerical simulations of the interaction of a pure TE soliton, and a pseudoscalar soliton for $Q_1 = 0.2$ and -0.2, respectively. Figure 14(a) shows an attractive interaction, while Fig. 14(b) shows a repulsive interaction. The results show that this may be a good way to control beam collapse and repulsion. In other words, upon switching the sign of the applied magnetic field, a potential barrier is switched on between the two beams. This may have a fundamental application in the magnetooptic nonlinear optics. In Fig. 15 we plot the collapse distance of a pure TE and a pseudoscalar soliton, as it varies with Q_1. This figure shows how the magnetic field can operate. Basically, the reversal of the field creates a new possibility for the collapse distance $Q_1 > 0$, for the forward direction, and the collapse distance increases as the field increases from zero ($Q_1 = 0$). Eventually an exponential increase sets in. For $Q_1 \geqslant 0.18$, a repulsive regime results, where the two beams continue, without hindrance, to exist, as shown in Fig. 14(b). For the negative direction of field

$Q_1<0$, the magnetic field draws the two solitons in, by reducing the collapse distance. These features alone suggest some device possibility, and that an interesting range of spatial soliton experiments can be anticipated.

V. CONCLUSIONS

Vector TE-TM waves in magneto-optic planar $\chi^{(2)}$ waveguides have a richer structure than scalar waves. The basic theory for them is derived here, and is expressed in the form of four coupled equations. In this paper, the first details concern the cascaded limit, when the system condenses to two coupled equations for the TE and TM waves. Different scalar and vector soliton solutions are obtained. The four coupled equations and then used to study the interactions of two pure TE solitons, and also the interaction of a TE soliton and a pseudoscalar soliton. The effect of an applied magnetic field is also investigated, and interesting repulsive and collapsing regimes, for interacting solitons are produced by switching the magnetic-field direction. It is concluded that planar waveguides using $\chi^{(2)}$ crystals and magnetic interfaces are going to be of great interest, because the potential applications look extremely promising.

ACKNOWLEDGMENTS

We would like to thank Professor Arnold of the University of Glasgow, UK for his considerable input. We must also acknowledge support from the UK Engineering and Physical Sciences Research Council (EPSRC).

[1] M. Schubert and B. Wilhelmi, *Nonlinear Optics and Quantum Electronics* (Wiley, New York, 1986).
[2] R. DeSalvo, D. J. Hagan, M. Sheik-Bahae, G. I. Stegeman, and E. W. Van Stryland, Opt. Lett. **17**, 28 (1992).
[3] C. R. Menyuk, R. Schiek, and L. Torner, J. Opt. Soc. Am. B **11**, 2434 (1994).
[4] A. G. Kalocsai and J. W. Haus, Opt. Commun. **97**, 239 (1993).
[5] A. G. Kalocsai and J. W. Haus, Phys. Rev. A **49**, 574 (1994).
[6] W. E. Torruellas, G. Krijnen, D. Y. Kim, R. Schiek, G. I. Stegeman, P. Vidakovic, and J. Zyss, Opt. Commun. **112**, 122 (1994).
[7] G. Assanto, I. Torelli, and S. Trillo, Opt. Lett. **19**, 1720 (1994).
[8] R. Schiek, J. Opt. Soc. Am. B **10**, 1848 (1993).
[9] L. Torner, C. R. Menyuk, and G. I. Stegeman, J. Opt. Soc. Am. B **12**, 889 (1995).
[10] A. V. Buryak and Y. S. Kivshar, Opt. Lett. **19**, 1612 (1994).
[11] A. V. Buryak and Y. S. Kivshar, Phys. Lett. A **197**, 407 (1995).
[12] A. V. Buryak and Y. S. Kivshar, Phys. Rev. A **51**, R41 (1995).
[13] A. D. Boardman, K. Xie, and A. Sangarpaul, Phys. Rev. A **52**, 4099 (1995).
[14] A. D. Boardman and K. Xie, Phys. Rev. A **50**, 1851 (1994).
[15] A. D. Boardman, K. Xie, and A. A. Zharov, Phys. Rev. A **51**, 692 (1995).
[16] A. D. Boardman and K. Xie, Radio. Sci. **28**, 891 (1993).
[17] A. D. Boardman and K. Xie, Phys. Rev. Lett. **75**, 4591 (1995).
[18] K. H. J. Buschow, in *Ferromagnetic Materials*, edited by E. P. Wohlfarth and K. H. J. Buschow (Elsevier Science Publishers, Amsterdam, 1988).
[19] W. H. Press, S. A. Teukdsky, W. T. Vetterling, and B. P. Flannery, *Numerical Recipes* (Cambridge University Press, Cambridge, 1992).